IEEE Access
Multidisciplinary | Rapid Review | Open Access Journal

Received April 23, 2020, accepted May 5, 2020, date of publication May 8, 2020, date of current version May 21, 2020.

Digital Object Identifier 10.1109/ACCESS.2020.2993317

Analytical Design of a Hybrid-Excited Wound Field Synchronous Machine for the Improvement of Torque Characteristics

WENPING CHAI, (Student Member, IEEE), JUNG-WOO KWON, AND BYUNG-IL KWON, (Senior Member, IEEE)
Department of Electronic Engineering, Hanyang University, Ansan 15588, South Korea

Corresponding author: Byung-il Kwon (bikwon@hanyang.ac.kr)

This work was supported in part by the Korea Institute of Energy Technology Evaluation and Planning (KETEP) and the Ministry of Trade, Industry and Energy (MOTIE) of the Republic of Korea under Grant 20174030201780, and in part by the BK21PLUS Program through the National Research Foundation of Korea within the Ministry of Education.

ABSTRACT This paper proposed a novel hybrid-excited wound field synchronous machine (HE-WFSM) to efficiently use the field torque and reluctance torque. Meanwhile, an analytical method is utilized to achieve the torque-angle consistency principle, which allows the field torque and the reluctance torque to reach their maximum values at the same phase current angle. First, a novel HE-WFSM with two different rotor excitations is proposed. Second, the PMs and the field windings in the rotor are designed by an analytical method based on the magnetic equivalent circuit (MEC) to produce the same magnetic flux in the air gap to obtain the torque-angle consistency. Third, one practical HE-WFSM applied for a small power fan is designed by the analytical method as an example. Finally, all the performances of the proposed HE-WFSM are predicted by the finite element method (FEM), thereby verifying the improved torque characteristics.

INDEX TERMS Wound field synchronous machine, hybrid excitation, reluctance torque, field torque.

I. INTRODUCTION

Wound field synchronous machines (WFSMs) are drawing increasing attention because they are not limited by a magnet and flexible flux regulation in various applications, such as electric vehicles [1], steam turbines [2], and wind turbines [3]. Nevertheless, the efficiency and torque/power density of a WFSM is generally lower than that of a permanent magnet synchronous machine (PMSM) because of the copper loss of the rotor winding and the brush system.

To overcome the disadvantages of conventional WFSMs, several topologies have been proposed to replace the brushes, slip rings, and exciter assembly [4]. Several topologies use permanent magnet (PM) to provide additional magnet torque [5]. Moreover, the saliency ratio, which is low in conventional WFSMs, has been improved by using a single air barrier, which contributes to the production of reluctance torque, resulting in high torque density and efficiency [6]. In an elegant *d-q* rotor frame equivalent circuit, the output torque of conventional WFSMs is a combination of the reluctance torque and field torque, each of which reaches its maximum value at different current phase angles that are 45 electrical degrees with respect to each other in theory [7]. When the maximum values of the reluctance and field torque are obtained near or at the same current phase angle, the torque density and efficiency can be enhanced [8]. This is generally known as the torque-angle approaching principle or the torque-angle consistency principle, which is widely used in interior PM motors [9], surface inset PM motors [10], PM-assisted synchronous reluctance motors [11], etc. Mostly, this principle is based on an asymmetrical rotor structure. Although the output average torque and the torque ripple may be improved by an asymmetrical rotor structure, problems such as that of unidirectional operation [12] could occur. Winzer and Doppelbauer have done the theoretical analysis of synchronous machines with displaced reluctance axis, which shows the PM can be effectively saved by the displaced angle [13]. Also [14] proposed a HE-WFSM with asymmetrical geometry to displace the reluctance axis by approximately 30 electrical degrees while avoiding a lower generating torque. This machine in [14]

The associate editor coordinating the review of this manuscript and approving it for publication was Atif Iqbal.

adheres to the torque-angle approaching principle, and the final version of the proposed rotor claims to be designed by optimization.

Moreover, optimization of the design, which is a popular method to achieve the above-mentioned principle, is complex and computationally expensive. A machine with the same topology but a different size would need to be optimized again. The essence of a machine design process is that it should allow fast, flexible, and accurate calculation of the machine characteristics. Several methods have been established to achieve and verify the required approaches. MEC is the most convenient and direct way to calculate the characteristics of a machine by using magnetic field analysis [15]. Especially, introducing MEC at an early stage of the design would make it possible to omit time-consuming processes such as optimization [16] and considering the overhang structure of an IPMM [17].

This paper proposes a novel HE-WFSM with a symmetrical PM-assisted structure to efficiently use the field torque and reluctance torque. And an analytical method is used to efficiently accomplish the design to enable the torque-angle consistency principle, such that the magnetic torque and the reluctance torque reach their maximum at the same current phase angle. The analytical design is based on the magnetic circuit model to reveal the working principle. Finally, the proposed HE-WFSM is analyzed with the aid of the FEM to verify the achievement of the torque-angle consistency principle. And the average torque as well as the efficiency of the machine are improved.

II. MACHINE TOPOLOGIES

A. THE CONVENTIONAL MACHINE

A conventional machine, applied in small power fan applications, is adopted as shown in Figure 1. The main specifications of the conventional machine are summarized in Table 1. The slot-pole combination of the machine is six slots and four poles. In this machine, the concentrated windings are adopted.

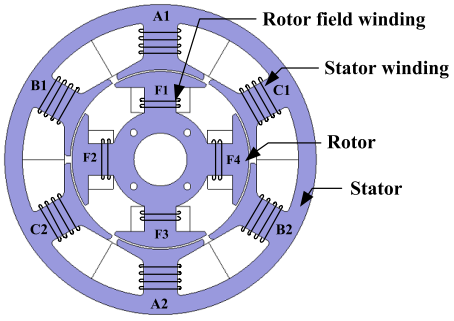

FIGURE 1. Structure of the conventional machine.

B. ELECTROMAGNETIC TORQUE EXPRESSION

Normally in d-q coordinates, the d-axis is defined as the magnetic direction produced by rotor excitation and the q-axis is positioned 90 electrical degrees counterclockwise from the d-axis. The electromagnetic torque can be obtained in the elegant d-q rotor equivalent circuit and expressed as:

$$T = \frac{3p}{2}\left[\lambda_f i_q + i_d i_q \left(L_d - L_q\right)\right] \tag{1}$$

where p is the number of pole pairs, L_d and L_q are the inductances of the d- and q-axes, respectively, $i_d = -i_s\, sin(\gamma)$ and $i_q = i_s\, cos(\gamma)$ are the current of the d- and q-axes, respectively, γ is the spatial angle of the stator current vector measured with respect to the q-axis and is also called as the current phase angle, i_s is the peak value of phase current and λ_f is the peak fundamental value of rotor flux linking the stator windings. The first term in (1) is termed the field torque, whereas the second is the reluctance torque. When WRSM with $L_d > L_q$ is controlled with 1st quadrant operation as shown in Figure 2 based on $-90° < \gamma < 0°$, the signs of the field and reluctance torques are equal [18]. The current angle difference is 45 electrical degrees between the maximum field torque and the maximum reluctance torque.

TABLE 1. Specifications of the conventional machine.

Item	Unit	Value
Rated current	A	1.6
Rated speed	rpm	1500
Stator outer diameter	mm	88
Air gap length	mm	0.5
Motor axial length	mm	52
Magnetic motive force	A*turns	0.75*100
Rotor pole arc	mech. deg	54
Rated torque	Nm	0.302

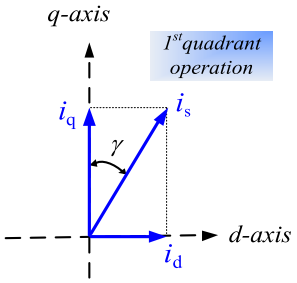

FIGURE 2. Current phasor diagram in the *d-q* frame.

C. THE PROPOSED HE-WFSM

To facilitate the design of the rotor total excitation flux direction, the novel structure of the proposed HE-WFSM is illustrated in Figure 3. For each rotor pole of the proposed HE-WFSM, two units of the spoke-type PMs are embedded symmetrically with the same magnetization direction. For the adjacent rotor poles, the PMs have the opposite magnetization direction. The rotor field winding is wound as

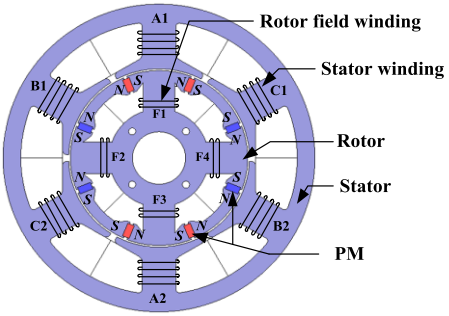

FIGURE 3. Structure of the proposed HE-WFSM.

the conventional one. The stator is the same as that of the conventional machine.

The excitations of the rotor in the proposed HE-WFSM are combined with PMs and field windings. The simplified rotor structure with each rotor excitation active is shown in Figure 4. Conventionally, the d-axis is aligned with the rotor flux linkage phasor depending on the direction of the total rotor magnetic flux. The salient pole of the proposed HE-WFSM is responsible for generating the reluctance torque. However, its d-axis is defined as the axis at which the greatest inductance appears in the rotor. This axis is always aligned with the rotor pole body. For the sake of distinction, it is referred to as the d_r-axis. When only field winding is active, the direction of the rotor flux linkage phasor is aligned to the rotor pole body, which is defined as $d_{winding}$. When only PM is active, the direction of the rotor flux linkage phasor is perpendicular to the $d_{winding}$, which is defined as d_{PM}. When field winding and PM are active at the same time, the direction of the total rotor magnetic flux is between the $d_{winding}$ and d_{PM}, which is defined as d_f. The displacement angle between d_r and d_f would be expected to improve the torque characteristics.

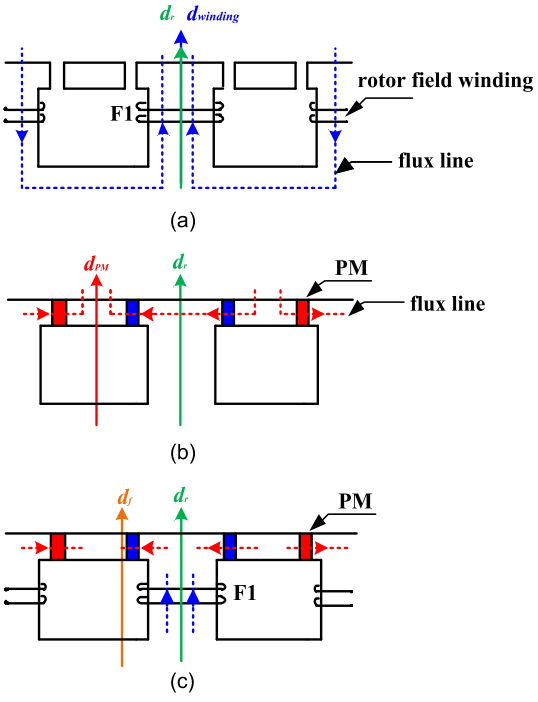

FIGURE 4. Simplified rotor structure (a) only field winding active (b) only PM active (c) field winding and PM active.

The air gap flux density distribution of the proposed HE-WFSM, shown in Figure 5, can be divided into two parts. The first part of the distribution is only produced by the field windings, and the other is only produced by the PMs. The amplitude of the air gap flux density produced by the field windings is defined as B_{field}, and the related angle is defined as θ_{field}. The amplitude of the air gap flux density produced by the PMs is defined as B_{PM}, and the related angle is defined as θ_{PM}. The air gap flux density distribution directly determines the characteristic of the proposed HE-WFSM, which is detailed in Section III.

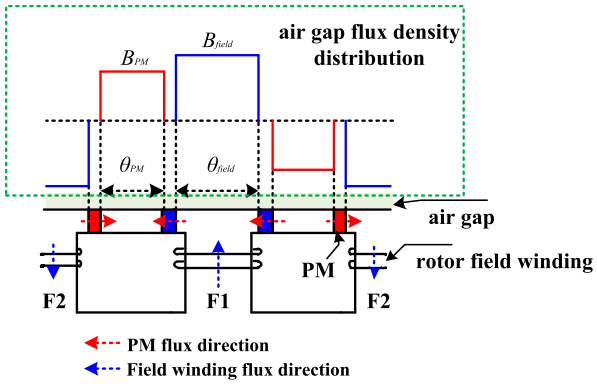

FIGURE 5. Theoretical air gap flux density distribution of the proposed HE-WFSM.

D. TORQUE-ANGLE CONSISTENCY PRINCIPLE

In the proposed HE-WFSM, the direction of the magnetic flux produced by the field winding is the same as the rotor pole body, and the direction of the magnetic flux produced by the PM is perpendicular to that produced by the rotor field winding. The direction of the rotor total magnetic flux is shown in Figure 6, in which δ is determined by the rotor field winding (including the number of turns and the current value) and the PM (including the PM volume and remanence).

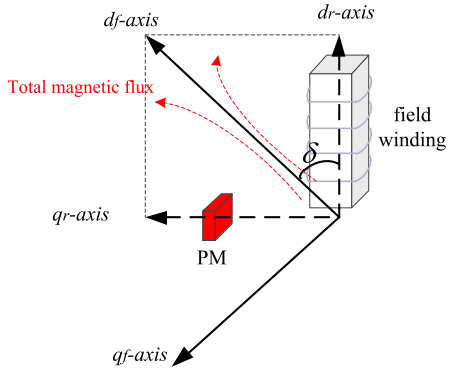

FIGURE 6. Definition of the *d-q* axis frame of the proposed HE-WFSM.

The d_r-q_r axis coordinate shown in Figure 6 is used to describe the generated reluctance torque. For the sake of distinction, the d_f-q_f axis coordinate shown in Figure 6 is used to describe the generated field torque.

In (1), the field torque term and the reluctance torque term should be in the same d-q axis coordinates. Here, the d_f-axis of the field torque is considered as the d-axis standard. Hence, the d_r-q_r axis coordinates should be shifted by δ electrical degrees. The electromagnetic torque in the d_f-q_f axis coordinates of the proposed HE-WFSM is concisely expressed as (2) by separating the field torque and the reluctance torque versus the current phase angle.

$$\begin{cases} T_{field} = T_{field\,\max} * \cos\gamma \\ T_{rel} = -T_{rel\,\max} * \sin 2(\gamma - \delta) \end{cases} \tag{2}$$

where $T_{field\ max}$ is the maximum absolute field torque and $T_{rel\ max}$ is the maximum absolute reluctance torque.

The curves of the torque components for the difference δ according to (2) are shown in Figure 7. The results show that, when δ is equal to 45°, the field torque and the reluctance torque would reach a maximum value at the same current phase angle.

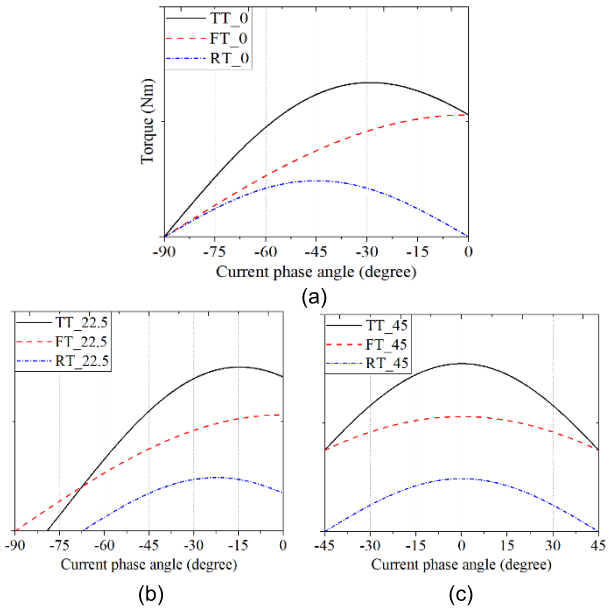

FIGURE 7. Torque components for different δ. TT: total torque, FT: field torque, RT: reluctance torque. (a) 0° (b) 22.5° (c) 45°.

According to Figure 6, when the magnetic flux produced by the rotor field winding is equal to the magnetic flux produced by the PMs, δ is equal to 45° and the torque-angle consistency principle can be achieved.

III. PREDICTION OF AIR GAP FLUX DENSITY DISTRIBUTION BY MEC

The air gap flux density distribution under the no-load condition directly reflects the magnetic flux produced by each excitation in the rotor, which is important in designing the δ in (2). To simplify the analytical design by MEC, the slotless air gap flux density distribution is adopted here.

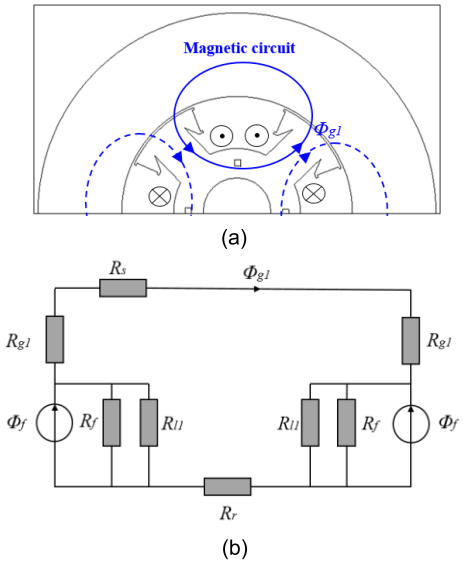

FIGURE 8. MEC of the proposed rotor type excited by the rotor field winding. (a) Flux path. (b) MEC.

The air gap flux density distribution of the HE-WFSM can be regarded as the superposition of the air gap flux density distribution generated by the rotor field windings and the PMs. Figure 8 (a) shows the flux path of the slotless HE-WFSM under one pole pair that is only produced by the field windings. Based on the magnetic circuit with a blue solid line, a simple MEC of the proposed HE-WFSM with only the field winding excitation is shown in Figure 8 (b). Due to the no-load condition, the local magnetic saturation can be assumed to be ignored. The air gap section is modeled by two magnetic reluctances with the same value (R_{g1}). The rotor field winding section is modeled by core magnetic reluctances (R_f) and flux sources (Φ_f). The section of the rotor pole ends is modeled by ending magnetic reluctances (R_{l1}). In addition, R_s is the magnetic reluctance of the stator back iron, R_r is the magnetic reluctance of rotor back iron, and Φ_{g1} is the flux passing through the air-gap in the rotor pole-arc range.

In order to simply the calculation process, the flux leakage is ignored. Hence, the amplitude of the air gap flux density B_{field} can be calculated by the following equations.

$$\Phi_{g1} = \frac{2 * F_f}{2 * R_{g1} + R_s + R_r + 2 * R_f} \tag{3}$$

$$F_f = N_f I_f \tag{4}$$

$$R_* = \frac{l_*}{\mu_0 u_{r*} A_*} \tag{5}$$

$$B_{field} = \frac{\Phi_{g1}}{A_{g1}} \tag{6}$$

where F_f is the rotor magnetic motive force; N_f is the number of turns of the rotor field winding; I_f is the current value of

the rotor field winding; R_* is the magnetic reluctance; l_* is the length of each path; μ_0 is the magnetic permeability of air; μ_{r*} *is* the relative magnetic permeability of the corresponding material; A_* is the cross-sectional area of the corresponding magnetic path; and $A_{g1=}\theta_{field} * r * L_a$ is the cross-sectional area of the air gap in the magnetic path, r is the radius of the air gap.

In addition, θ_{field} determines the distribution angle of the amplitude of the air gap flux density produced by the rotor field windings. Therefore, the slotless air gap flux density distribution contributed by the rotor field windings is shown in Figure 9. The FEM result confirms the reliability of the MEC result.

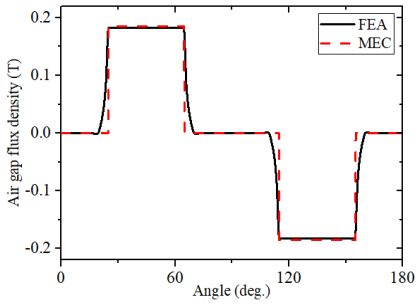

FIGURE 9. Slotless air gap flux density with field winding excitation.

Figure 10 (a) shows the flux path of the slotless HE-WFSM under one pole pair that is only produced by the PMs. According to the magnetic circuit with a red solid line, a simple MEC of the proposed HE-WFSM with only the PM excitation is shown in Figure 10 (b). The magnetic saturation and the effect of irreversible demagnetization of the PM are not considered. The air gap section is modeled by four magnetic reluctances with the same value (R_{g2}). The PM sections are modeled by the core magnetic reluctances (R_m) and flux sources (Φ_{pm}). The section containing the rotor pole ends is modeled by the ending magnetic reluctances (R_{l2}). R_{s2} is the magnetic reluctance of the stator back iron. R_{r2} is the magnetic reluctance of the rotor back iron. Φ_{g2} is the flux passing through the air-gap in the rotor pole-arc range.

To simplify the calculation process, the flux leakage is ignored. Hence, the amplitude of the air gap flux density B_{PM} can be calculated by the following equations.

$$\Phi_{pm} = B_r w_{pm} L_a \tag{7}$$

$$\Phi_{g2} = \frac{R_m}{2 * R_{g2} + R_{s2} + R_{r2} + R_m} \Phi_{pm} \tag{8}$$

$$B_{PM} = \frac{\Phi_{g2}}{A_{g2}} \tag{9}$$

where B_r represents the remanence flux density of the PM; w_{pm} is the thickness of the PM block; L_a is the axis length of the PM; and $A_{g2} = \theta_{PM} * r * L_a$ is the cross-sectional area of the air gap in the magnetic path.

In addition, θ_{PM} determines the distribution angle of the amplitude of the air gap flux density produced by the PMs.

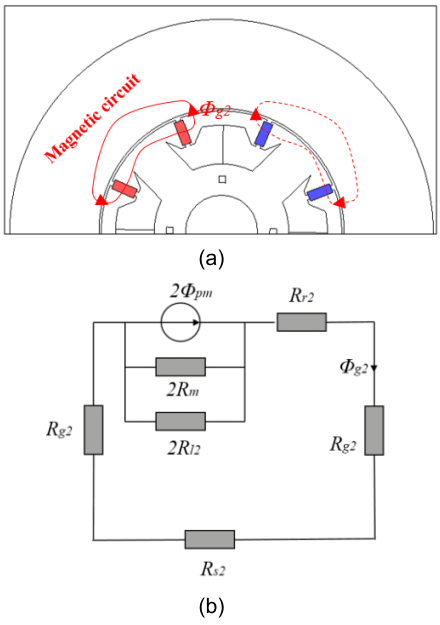

FIGURE 10. MEC of the proposed rotor type excited by PMs: (a) Flux path, (b) MEC.

Therefore, the slotless air gap flux density distribution contributed by the PMs is shown in Figure 11. The FEM result confirms the reliability of the MEC result.

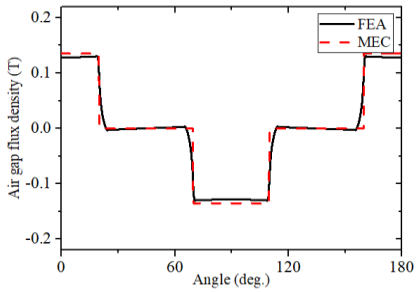

FIGURE 11. Slotless air gap flux density with excitation of the PMs.

Consequently, the resultant slotless air-gap flux density is obtained as the vector sum of the two components, and is shown in Figure 12. The FEM result verifies that the results obtained with the analytical method are reliable, indicating that the analytical method can be used to design the slotless air-gap flux density distribution of the proposed HE-WFSM.

In this analytical design, the magnetic flux produced by the rotor field winding is expressed as $B_{field}A_{g1}$, and that produced by the PMs is expressed as $B_{PM}A_{g2}$. According to the discussion in section II.D, $B_{field}A_{g1} = B_{PM}A_{g2}$ ensures to achieve $\delta = 45°$ as the torque-angle consistency principle.

IV. SIMULATION AND EVALUATION

To verify the effectiveness of the analytical design for the novel HE-WFSM to achieve the torque-angle consistency principle, a practical HE-WFSM is designed with the aid of MATLAB. The parameters obtained in this calculation are listed in Table 2. Jmag-designer software was employed to

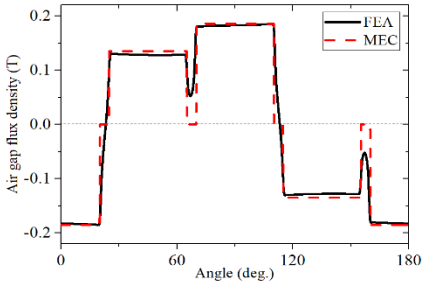

FIGURE 12. Slotless air gap flux density of the proposed HE-WFSM.

TABLE 2. The designed parameters related to the rotor excitations.

Item	Unit	Value
Number of turns of the field winding	-	90
Current value of field winding	A	0.75
Remanence of PMs	T	0.47
PM volume	mm^3	3244.8

build the FEM model to extensively confirm electromagnetic performance.

A. AIR GAP FLUX DENSITY

The air gap flux densities of the conventional machine and the designed HE-WFSM are predicted by MEC and FEM as shown in Figure 13, which confirms the designed parameters related to the rotor by MEC are reliable. The results are consistent with the previous theoretical analysis in Section II.D. This confirms that the MEC could assist motor designers to determine the expected air gap flux density more accurately and efficiently.

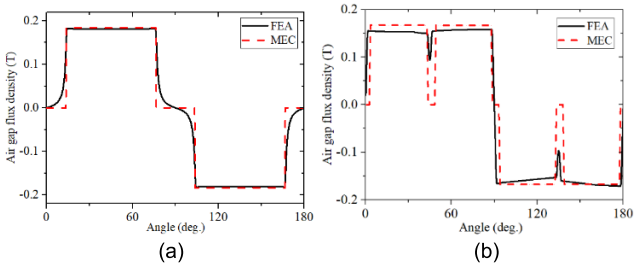

FIGURE 13. Slotless air-gap flux density distribution (a) the conventional machine (b) the designed HE-WFSM.

The magnetic flux density distributions including the color-bar for the conventional machine and the designed HE-WFSM under the study in FEM are shown in Figure 14.

B. BACK-EMF

The simulated back-EMFs and their FFT results for the conventional machine and the designed HE-WFSM are presented in Figure 15 and Figure 16, respectively. The number of

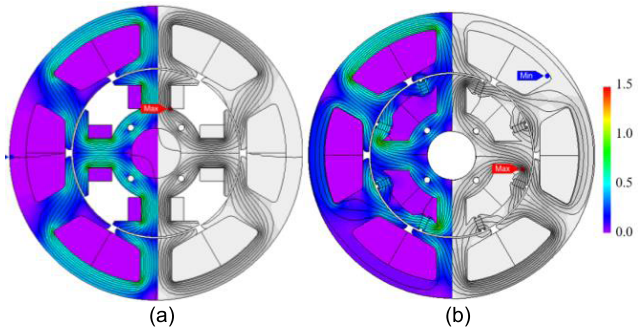

FIGURE 14. Magnetic flux density distribution (a) the conventional machine (b) the designed HE-WFSM.

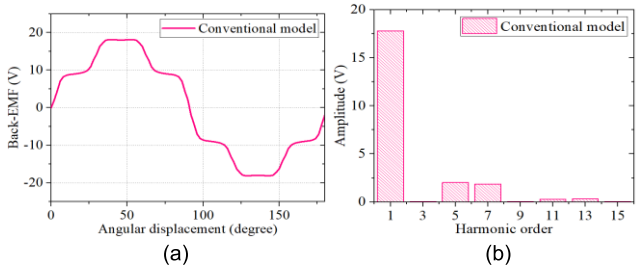

FIGURE 15. Back-EMF of the conventional machine (a) waveform (b) FFT.

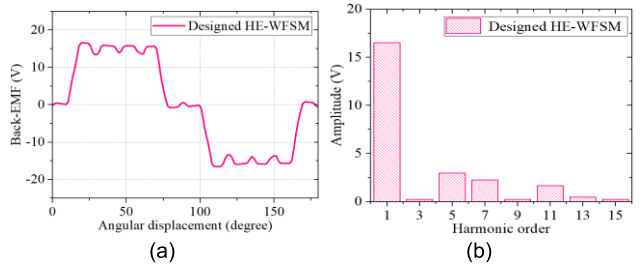

FIGURE 16. Back-EMF of the designed HE-WFSM (a) waveform (b) FFT.

turns of the rotor field windings of the designed HE-WFSM is reduced by 10% compared with that of the conventional machine. In contrast, the fundamental component of the back-EMF of the designed HE-WFSM is only reduced by 7.2% with the help of the assisted PM and its RMS is reduced by 4.1%, compared with that of the conventional machine. However, the total harmonic distortion (THD) is increased from 15.5% to 25.0%.

C. TORQUE COMPONENT CHARACTERISTICS

The frozen permeability method is applied to segregate the torque into its reluctance and field torque components to evaluate the contribution of the designed HE-WFSM [19]. Here, the field torque is defined as the difference between the total torque and the reluctance torque.

The torque characteristics of the conventional machine and the designed HE-WFSM with respect to the current phase angles are displayed in Figure 17. The results indicate that the magnetic torque and reluctance torque of the

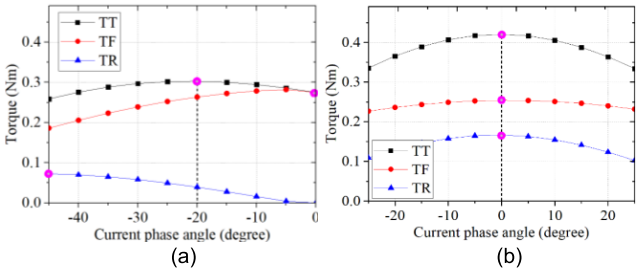

FIGURE 17. Torque varies with the current angle (a) the conventional machine (b) the designed HE-WFSM.

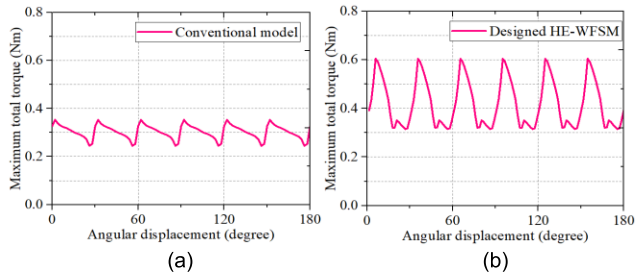

FIGURE 18. Electromagnetic torque (a) the conventional machine (b) the designed HE-WFSM.

TABLE 3. The designed parameters related to the rotor excitations.

Item	Unit	Conventional machine	Designed HE-WFSM
Back-EMF (RMS)	V	12.68	12.16
Max. total torque	Nm	0.302	0.421
Max. reluctance torque	Nm	0.071	0.167
Utilized reluctance torque	Nm	0.048	0.167
Max. field torque	Nm	0.273	0.254
Utilized field torque	Nm	0.254	0.254
Torque ripple	%	35.68	68.82
Efficiency	%	85.5	89.1

conventional machine reach their maximum values at current phase angles that differ by 45 electrical degrees, whereas these two torque components of the designed HE-WFSM reach maximum values at the same current phase angle as predicted. Thus, the torque-angle consistency principle has been verified. The results show that the average values of the maximum total torque and the utilized reluctance torque in the designed HE-WFSM are greatly increased by 39.4% and 247.9%, respectively, compared with those of the conventional machine.

Figure 18 shows the electromagnetic torque waveforms of the conventional machine and the designed HE-WFSM. Even though the torque ripple of the designed HE-WFSM is worse, this would not be overly problematic for applications in which torque ripple is not strictly required. The analysis shows that the efficiency of the designed HE-WFSM at maximum torque has increased by 4.2% compared with that of the conventional machine. The numerical results are summarized in Table 3.

V. CONCLUSION

This paper proposed a novel HE-WFSM to achieve to efficiently use the field torque and reluctance torque. Meanwhile, the analytical method has been utilized to efficiently design to allow the field torque and the reluctance torque to reach their maximum at the same phase current angle. A small HE-WFSM was designed by the analytical method and verified as an example. The calculations showed that the maximum total torque and efficiency of the designed HE-WFSM are improved by 39.4% and 4.2%, respectively, compared with those of the conventional model. It is worth mentioning that the torque of the designed HE-WFSM is increased at the expense of higher torque ripple. As a future direction, we plan to further improve the analytical design of the HE-WFSM by considering the torque, efficiency, and torque ripple all together to meet the requirements of most applications.

REFERENCES

[1] A. Di Gioia, I. P. Brown, Y. Nie, R. Knippel, D. C. Ludois, J. Dai, S. Hagen, and C. Alteheld, "Design and demonstration of a wound field synchronous machine for electric vehicle traction with brushless capacitive field excitation," *IEEE Trans. Ind. Appl.*, vol. 54, no. 2, pp. 1390–1403, Mar. 2018.

[2] L. Weili, W. Purui, L. Yong, X. Yi, L. Dong, Z. Xiaochen, and Z. Jianjun, "Influence of rotor structure on field current and rotor electromagnetic field of turbine generator under out-of-phase synchronization," *IEEE Trans. Magn.*, vol. 53, no. 6, pp. 1–4, Jun. 2017.

[3] N. S. Hasan, M. Y. Hassan, M. S. Majid, and H. A. Rahman, "Review of storage schemes for wind energy systems," *Renew. Sustain. Energy Rev.*, vol. 21, pp. 237–247, May 2013.

[4] D. C. Ludois, J. K. Reed, and K. Hanson, "Capacitive power transfer for rotor field current in synchronous machines," *IEEE Trans. Power Electron.*, vol. 27, no. 11, pp. 4638–4645, Nov. 2012.

[5] S.-W. Hwang, J.-H. Sim, J.-P. Hong, and J.-Y. Lee, "Torque improvement of wound field synchronous motor for electric vehicle by PM-assist," *IEEE Trans. Ind. Appl.*, vol. 54, no. 4, pp. 3252–3259, Jul. 2018.

[6] W. Chai, W. Zhao, and B.-I. Kwon, "Optimal design of the wound field synchronous reluctance machines to improve torque by increasing saliency ratio," *IEEE Trans. Magn.*, vol. 53, no. 11, pp. 1–4, Nov. 2017.

[7] G. Xu, G. Liu, W. Zhao, Q. Chen, and X. Du, "Principle of torque-angle approaching in a hybrid rotor permanent-magnet motor," *IEEE Trans. Ind. Electron.*, vol. 66, no. 4, pp. 2580–2591, Apr. 2019.

[8] W. Zhao, H. Shen, T. A. Lipo, and X. Wang, "A new hybrid permanent magnet synchronous reluctance machine with axially sandwiched magnets for performance improvement," *IEEE Trans. Energy Convers.*, vol. 33, no. 4, pp. 2018–2029, Dec. 2018.

[9] X. Zeng, L. Quan, X. Zhu, L. Xu, and F. Liu, "Investigation of an asymmetrical rotor hybrid permanent magnet motor for approaching maximum output torque," *IEEE Trans. Appl. Supercond.*, vol. 29, no. 2, Mar. 2019, Art no. 0602704.

[10] W. Zhao, T. A. Lipo, and B.-I. Kwon, "Optimal design of a novel asymmetrical rotor structure to obtain torque and efficiency improvement in surface inset PM motors," *IEEE Trans. Magn.*, vol. 51, no. 3, Mar. 2015, Art no. 8100704.

[11] F. Xing, W. Zhao, and B.-I. Kwon, "Design and optimisation of a novel asymmetric rotor structure for a PM-assisted synchronous reluctance machine," *IET Electr. Power Appl.*, vol. 13, no. 5, pp. 573–580, May 2019.

[12] R. Hamdy, J. Fletcher, and B. W. Williams, "Bidirectional starting of a symmetrical two-phase switched reluctance machine," *IEEE Trans. Energy Convers.*, vol. 15, no. 2, pp. 211–217, Jun. 2000.

[13] P. Winzer and M. Doppelbauer, "Theoretical analysis of synchronous machines with displaced reluctance axis," in *Proc. Int. Conf. Electr. Mach. (ICEM)*, Sep. 2014, pp. 641–647.

[14] P. Winzer and M. Doppelbauer, "A hybrid permanent magnet and wound field synchronous machine with displaced reluctance axis capable of symmetric four quadrant operation," in *Proc. 18th Eur. Conf. Power Electron. Appl. (EPE ECCE Europe)*, Sep. 2016, pp. 1–11.

[15] J.-J. Lee, J. Lee, and K.-S. Kim, "Design of a WFSM for an electric vehicle based on a nonlinear magnetic equivalent circuit," *IEEE Trans. Appl. Supercond.*, vol. 28, no. 3, pp. 1–4, Apr. 2018.
[16] Y. Liu, M. Zhang, Y. Zhu, J. Yang, and B. Chen, "Optimization of voice coil motor to enhance dynamic response based on an improved magnetic equivalent circuit model," *IEEE Trans. Magn.*, vol. 47, no. 9, pp. 2247–2251, Sep. 2011.
[17] H.-K. Yeo, D.-K. Lim, and H.-K. Jung, "Magnetic equivalent circuit model considering the overhang structure of an interior permanent-magnet machine," *IEEE Trans. Magn.*, vol. 55, no. 6, Jun. 2019, Art no. 8201404.
[18] M.-S. Lim and J.-P. Hong, "Design of high efficiency wound field synchronous machine with winding connection change method," *IEEE Trans. Energy Convers.*, vol. 33, no. 4, pp. 1978–1987, Dec. 2018.
[19] G.-J. Li, G. Jewell, and Z.-Q. Zhu, "Performance investigation of hybrid excited switched flux permanent magnet machines using frozen permeability method," *IET Electr. Power Appl.*, vol. 9, no. 9, pp. 586–594, Nov. 2015.

WENPING CHAI (Student Member, IEEE) was born in Liaoning, China, in 1991. She received the B.S. degrees in electrical engineering and automation, and also management from the Harbin Institute of Technology, in 2014. She is currently pursuing the Ph.D. degree in electrical engineering with the Department of Electrical and Electronic Engineering, Hanyang University, Ansan, South Korea. Her research interest includes the design, analysis, and optimization of electric machines.

JUNG-WOO KWON was born in 1992. He received the B.S. degrees in bio-nano engineering and electrical engineering, and the M.S. and Ph.D. degrees from Hanyang University, Ansan, South Korea, in 2015 and 2019, respectively. He is currently working as a Postdoctoral Researcher with the Department of Electrical and Electronic Engineering, Hanyang University. His research interest includes electric machines, especially on motors.

BYUNG-IL KWON (Senior Member, IEEE) was born in 1956. He received the B.S. and M.S. degrees in electrical engineering from Hanyang University, Ansan, South Korea, in 1981 and 1983, respectively, and the Ph.D. degree in electrical engineering and machine analysis from the University of Tokyo, Tokyo, Japan, in 1989.

From 1989 to 2000, he was a Visiting Researcher with the Faculty of Science and Engineering Laboratory, University of Waseda, Tokyo. In 1990, he was a Researcher with the Toshiba System Laboratory, Yokohama, Japan. In 1991, he was a Senior Researcher with the Institute of Machinery and Materials Magnetic Train Business, Daejeon, South Korea. From 2001 to 2008, he was a Visiting Professor with the University of Wisconsin–Madison, Madison, WI, USA. He is currently a Professor with Hanyang University. His research interest includes the design and control of electric machines.